

Relax, estimate, and track: a simple battery state-of-charge and state-of-health estimation method

Shida Jiang^a, Junzhe Shi^a, Scott Moura^a

^a*Department of Civil and Environmental Engineering, University of California, Berkeley, Berkeley, 94720, CA, USA*

Abstract

Battery management is a critical component of ubiquitous battery-powered energy systems, in which battery state-of-charge (SOC) and state-of-health (SOH) estimations are of crucial importance. Conventional SOC and SOH estimation methods, especially model-based methods, often lack accurate modeling of the open circuit voltage (OCV), have relatively high computational complexity, and lack theoretical analysis. This study introduces a simple SOC and SOH estimation method that overcomes all these weaknesses. The key idea of the proposed method is to momentarily set the cell's current to zero for a few minutes during the charging, perform SOC and SOH estimation based on the measured data, and continue tracking the cell's SOC afterward. The method is based on rigorous theoretical analysis, requires no hyperparameter fine-tuning, and is hundreds of times faster than conventional model-based methods. The method is validated on six batteries charged at different C rates and temperatures, realizing fast and accurate estimations under various conditions, with a SOH root mean square error (RMSE) of around 3% and a SOC RMSE of around 1.5%.

Keywords: Battery management system, state-of-charge, state-of-health, electric vehicle

1. Introduction

Battery management is crucial for the operational efficiency, safety, reliability, and cost-effectiveness of ubiquitous battery-powered energy systems, such as electrified vehicles and smart grids with renewables [1]. Among different goals of battery management systems (BMS), battery state-of-charge (SOC) and state-of-health (SOH) estimation are of crucial importance and

are directly related to accurate and efficient monitoring of the state information of power batteries [2].

Battery SOC describes the actual energy level available at the battery and is defined as the ratio of the present available capacity to the present maximum capacity. On the other hand, battery SOH reflects the aging state of the battery and is defined as the ratio of the present maximum cell capacity (or present cell resistance) to its initial value [3]. Considering that the battery’s internal resistance also changes as the battery is charged or discharged, we used the capacity version of the SOH definition in this paper. Namely, an 80% SOH means that the cell’s maximum capacity has decreased by 20%. The main difference between the SOC and the SOH is that SOC indicates the instant status of the battery, while SOH indicates the long-term dynamic status of the battery [4].

Many different methods have been proposed for SOC and SOH estimation. In general, these methods can be divided into three categories: direct measurement-based methods, model-based methods, and data-driven methods. Direct measurement-based methods estimate the SOC and SOH through directly measurable features like voltage, current, and resistance. These methods generally have low computational complexity. However, they either have low accuracy (e.g., resistance method) or can be only used offline (e.g., ampere-hour counting method and impedance method) [5]. The only exceptions are the differential voltage method and its variant incremental capacity method, using which many studies got pretty good SOC and SOH estimation results [6, 7, 8]. The “differential voltage” stands for the derivative of the terminal voltage with respect to the capacity, and the “incremental capacity” stands for the derivative of capacity with respect to the terminal voltage. These two methods estimate the SOC and SOH by extracting related features from the differential voltage or incremental capacity curves. The limitation of these two methods is that they require precise voltage measurement, and they only work when the current is constant and is lower than a specific value [9].

On the other hand, data-driven methods estimate the battery SOC and SOH by training a black-box model with a large dataset [10]. The input of the data-driven methods is usually health indicators derived from capacity, resistance, voltage, current, and temperature data [11]. The benefits of data-driven methods are that they do not need physical-based models and can have high accuracy [12]. The disadvantages are that they need high computational effort and are sensitive to the quantity and quality of training data [3].

Meanwhile, model-based methods estimate the SOC and SOH by first building a battery model to fit the raw data, and then, they use some model parameters to calculate the SOC and SOH indirectly. The battery model can either be a pure mathematical model or a battery equivalent circuit model (ECM) [4], whose purpose is to model the battery’s voltage response to any input current. In model-based methods, SOC is usually estimated based on the state-space function and the SOC-OCV correlation. At the same time, SOH estimation can be done by using another filter or by calculating the derivative of SOC [13, 14, 15]. In general, the accuracy of model-based methods depends on the model’s accuracy. With the help of adaptive filter algorithms such as a nonlinear Kalman filter (KF), model-based methods can usually achieve good accuracy compared to other methods [16]. The drawback is that the imperfection of the models often results in bias in the estimation, producing unexpected estimation errors.

However, although hundreds of different methods have been proposed for battery SOC and SOH estimation, we noticed that the existing methods have some common weaknesses. The first weakness is that, although the OCV-SOC correlation is widely used in SOC and SOH estimation, such correlation is also affected by temperature [17, 18, 19] and SOH [20, 21]. Yet, such influence (especially the effect of SOH) is constantly ignored in most studies. Such a simplification can be problematic because the OCV-SOC correlation function stored in the BMS will become increasingly inaccurate as the cell ages, making the SOC and SOH estimation results unreliable. Unfortunately, to the best of our knowledge, so far, only a few papers considered the effect of SOH when using the OCV-SOC correlation to estimate the SOC [22, 23, 24, 25]. Worse still, in [22], the authors only showed the correlation between some parameters and SOH, yet no SOH estimation method was proposed or validated; in [23], the primary focus was only SOC and OCV, and the SOH estimation result was not detailed; in [24], although a SOH estimation method was proposed, the method requires to fit the present OCV curve in an extensive SOC range (from 10% to 90%), which is hardly accessible in most applications; and in [25], the proposed method required fine-tuning some hyperparameters and was only validated at 100% and 96% SOH, so its effectiveness still requires further investigation. In summary, while many papers used the OCV-SOC correlation to estimate the SOC and SOH, few have developed an effective way to integrate the effect of battery aging on OCV into their method.

Another weakness of the existing battery SOC and SOH estimation meth-

ods is that little attention has been paid to reducing their computational complexity. In most studies, estimation accuracy is set to be the only metric used to measure how good or bad a method is. However, for state estimation of the battery pack, the computational complexity can also be an essential and practical factor to consider [26]. For example, in a Tesla Model S, there are 96 series-connected battery modules, so the workload and computational cost can be very high if we adopt a complex filter-based method for each module [27]. To solve such a problem, we noticed that some studies proposed to use a simple method first to identify the “weakest” cell in the battery pack (i.e., the cell that has the lowest voltage or some other apparent characteristics that make it more likely to have the lowest SOC or SOH) and then use another complex method to estimate the state of those weakest cells [27, 28, 29, 30]. While this idea can partially solve the question, the method may not capture the weakest cell correctly, which could make the estimation too optimistic.

Furthermore, most SOC and SOH estimation methods so far only use experimental data for validation and do limited theoretical analysis. While empirical data may be enough to verify the method’s effectiveness in one specific setting, such effectiveness can no longer be guaranteed once any setting (e.g., the sampling frequency of the voltmeter, the parameters of the ECM) changes. In the worst case, the algorithm may not even converge when the initial value is not accurate enough or when the measurement is not precise enough [10]. For example, the differential voltage method often uses a filter to reduce voltage measurement noise. However, in most papers that use this method so far, the noise filtering algorithm is only proposed empirically [6, 7, 8], so it may not work well when the precision of the voltmeter is lower. For another example, the extended Kalman filter (EKF) and unscented Kalman filter (UKF) are often used for SOC and SOH estimation. However, since no theoretical analysis is done to guarantee their convergence in SOH estimation [31], it is unclear whether the method can always yield satisfactory results as the battery ages.

In this paper, we proposed a novel model-based SOC and SOH estimation method that addresses all three weaknesses described above. The main contributions of this paper are:

- We proposed a SOC and SOH estimation method that can be easily implemented without any sophisticated device. Additionally, the estimation accuracy of the proposed method is pretty high, with a SOH

root mean square error (RMSE) of around 3% and a SOC RMSE of around 1.5%.

- To implement the method, the battery pack only needs to relax for one to four minutes during the charging process, which will not cause a significant delay. Besides, the computational complexity of our method is extremely low, making it suitable for online applications such as electric vehicles.
- The proposed method has no hyperparameter and does not require initialization. The noise tolerance and the convergence of the method are guaranteed by detailed theoretical analysis.

The paper is organized as follows. Section 2 introduces the definition of OCV, SOC, and SOH used in the paper. Section 3 presents the details of our SOC and SOH estimation method. Section 4 provides the theoretical basis of our method. Section 5 presents the experimental results and compares our method against UKF. A detailed analysis of the estimation error is also given in Section 5. Finally, in Section 6, we discuss the conclusion drawn from the study.

2. SOC, SOH, and OCV

2.1. Definition of SOC and SOH

The battery SOC is defined as:

$$SOC = \frac{Q_r}{Q} \quad (1)$$

where Q is the present maximum capacity of the battery, and Q_r is the remaining capacity of the battery.

The derivative form of (1), which is often used for SOC estimation, is:

$$\frac{dSOC}{dt} = \frac{I}{Q} \quad (2)$$

On the other hand, the battery SOH is defined as:

$$SOH = \frac{Q}{Q_0} \times 100\% \quad (3)$$

where Q_0 is the maximum capacity of a new cell.

It is worth mentioning that a cell’s capacity varies at different C rates. For the rigor of the definition, all the “capacity” above refers to the charge capacity (calculated by Coulomb counting) when the C rate is 0.1 C.

2.2. OCV model

In this study, the OCV curves were fitted by a ninth-order polynomial function due to its simplicity and low RMS error [32].

$$OCV = f(SOC, SOH, T) = \sum_{i=0}^9 a_i(SOH, T) SOC^i \quad (4)$$

where $a_i, i = 0, 1, \dots, 9$ are coefficients related to SOH and temperature (denoted by T in the equation). These coefficients can be determined by fitting the OCV curve of the battery.

There are generally two ways to acquire the OCV curve in experiments. The first is the slow-current OCV test, and the second is the incremental OCV test. In a slow-current OCV test, the cell is fully discharged and then fully charged at a constant current that is lower or equal to 0.1 C. On the other hand, in an incremental capacity test, the cell is usually charged and discharged with a higher C rate (e.g., 0.5 C). Whenever the SOC rises or drops by a certain percentage (e.g., 10%), the cell is open-circuited for some time (e.g., two hours) [33]. Compared with the low-current OCV test, the incremental capacity test can describe the battery behavior better [33] and make model-based SOC estimation more accurate [34]. As a result, in this study, incremental OCV tests are used to acquire the OCV-SOC curve. The OCV curve acquired from fitting the experimental data at 25°C is presented in Figure 1.

Note that the OCV curve in Figure 1 is only used in the theoretical analysis in Section 4.2 and never used in the experimental validation in Section 5. In the experimental validation, when the estimation is validated on a particular cell, that cell’s OCV data will be excluded when fitting the OCV curve. The purpose is to separate the data used for fitting the OCV curve and the data used for experimental validation.

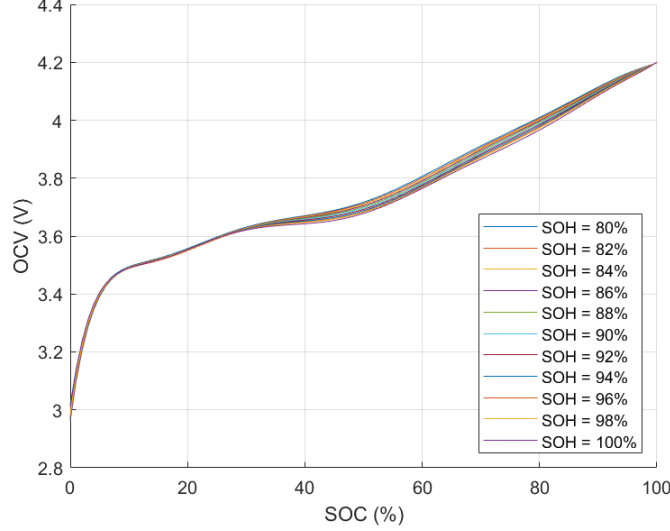


Figure 1: The fitted OCV curve at 25°C

3. Methodology

3.1. ECM model and parameter estimation

Since the SOH changes much more slowly than SOC, it can be considered constant during a single cycle. With this simplification and the definition of SOH in (3), when the temperature is constant, (2) can be rewritten as follows:

$$SOH = \frac{I}{Q_0} \frac{dt}{dSOC} = \frac{I}{Q_0} \frac{\partial OCV}{\partial SOC} \frac{dt}{dOCV} \quad (5)$$

(4) and (5) are two independent equations about SOC and SOH. With these two equations, we can solve the value of SOC and SOH once we know the values of OCV and $dOCV/dt$. However, OCV is not directly measurable unless the battery is idle for hours, so an ECM is required to estimate this parameter. The ECM used in this paper is presented in Figure 2. Despite the OCV, it consists of a resistor and an RC pair (a resistor and a capacitor connected in parallel).

If we select SOC and capacitor voltage (U_c) as the states, current (I) as the input, and terminal voltage (U_{ter}) as the output, the state-space function of the model can be written as

$$\begin{bmatrix} \dot{SOC} \\ \dot{U}_c \end{bmatrix} = \begin{bmatrix} 0 & 0 \\ 0 & \frac{-1}{R_2 C} \end{bmatrix} \begin{bmatrix} SOC \\ U_c \end{bmatrix} + \begin{bmatrix} \frac{1}{Q} \\ \frac{1}{C} \end{bmatrix} I \quad (6)$$

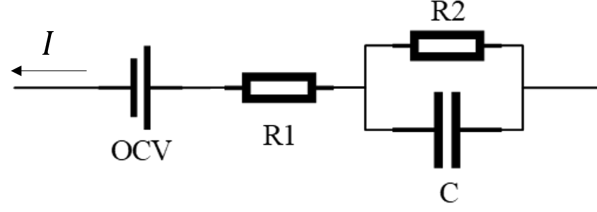


Figure 2: Battery equivalent circuit model

$$U_{ter} = OCV(SOC, SOH, T) + U_c + R_1 I \quad (7)$$

where R_1 , R_2 , and C are the ECM parameters shown in Figure 2.

Suppose that at time t_0 , the current suddenly drops to zero, then the output function becomes

$$U_{ter}(t_0 + \Delta t) = OCV(SOC, SOH, T) + U_c(t_0)e^{-\frac{\Delta t}{RC}}, \Delta t > 0 \quad (8)$$

If the current before t_0 was constant (denoted as I_0) and the capacitor had already reached steady-state, then

$$U_c(t_0) = I_0 R_2 \quad (9)$$

As for the parameter R_1 , its value can be estimated by using the equation below

$$R_1 = -\Delta U / I_0 \quad (10)$$

where ΔU is the sudden change in voltage after the current becomes zero.

Given (8), (9), and (10), all the parameters in the ECM can be estimated based on the measurement data. Namely, R_1 can be directly calculated by (10), and the other three parameters can be estimated using algorithms like regression analysis or parameter observer. However, these algorithms are quite complex (if we want them to be robust to noise) and unsuitable for cell-level or module-level estimation in a large battery pack with thousands of cells and around a hundred modules. Consequently, a more straightforward parameter estimation method is used in this paper to estimate the other three ECM parameters, which is to determine the three parameters by using three data points. Namely, given three pairs of time and terminal voltage data (x_1, y_1) , (x_2, y_2) , and (x_3, y_3) , the parameters can be determined by solving

the following function set

$$\begin{cases} y_1 = OCV + I_0 R_2 e^{-\frac{x_1}{R_2 C}} \\ y_2 = OCV + I_0 R_2 e^{-\frac{x_2}{R_2 C}} \\ y_3 = OCV + I_0 R_2 e^{-\frac{x_3}{R_2 C}} \end{cases} \quad (11)$$

where x_1, x_2, x_3 are counted after the relaxation starts.

To improve the noise tolerance of the method, the selection of the three points must be optimized. Otherwise, a small noise in the measurement can make the parameter inaccurate. For this purpose, the general rule of thumb is to select a small x_1 , a big x_3 , and select $x_2 = \frac{x_1 + x_3}{2}$. The theoretical analysis behind this rule is illustrated in Section 4.1. Following this rule, if we denote $x_3 - x_2 = x_2 - x_1 = x_d$, then (11) can be rewritten as:

$$\begin{cases} R_2 = \frac{(y_1 - y_2)e^{x_d/\tau}}{I_0(e^{x_d/\tau} - 1)} \\ C = \frac{\tau}{R_2} \\ OCV = y_1 - \frac{(y_1 - y_2)e^{x_d/\tau}}{e^{x_d/\tau} - 1} \end{cases} \quad (12)$$

where $\tau = \frac{x_d}{\ln \frac{y_1 - y_2}{y_2 - y_3}}$, and its physical meaning is the time constant of the RC pair.

Based on (12), the values of the three parameters can be directly calculated once the three data points are acquired. However, even if the three points have been optimized, estimating three parameters using three data points is still inevitably vulnerable to measurement noise. Therefore, to further improve the noise tolerance, it is necessary to filter out the noise before doing parameter estimation. The algorithm we chose here is a 15-point median filter, which replaces the voltage of each of the three points with the median value of the fifteen points adjacent to it (including itself). We chose this algorithm instead of other common filtering algorithms like averaging for two reasons. First, this algorithm is straightforward and only adds a little extra computational complexity. Secondly, we can theoretically prove that this filtering algorithm can always reduce the variance of the noise. In contrast, other algorithms only work when the variance of the noise is in a specific range. Namely, we have the following theorem.

Theorem 1. *If $x_1 > x_2$, yet the estimation of x_1 (denoted as \hat{x}_1), is smaller than the estimation of x_2 (denoted as \hat{x}_2), then swapping the two estimations can make the overall RMS error lower.*

Proof. After swapping, the change in mean square error is

$$\begin{aligned} & 0.5[(x_1 - \hat{x}_2)^2 + (x_2 - \hat{x}_1)^2] - 0.5[(x_1 - \hat{x}_1)^2 + (x_2 - \hat{x}_2)^2] \\ &= 0.5(-2\hat{x}_2x_1 - 2\hat{x}_1x_2 + 2\hat{x}_1x_1 + 2\hat{x}_2x_2) \\ &= (\hat{x}_1 - \hat{x}_2)(x_1 - x_2) < 0 \end{aligned}$$

Meaning that the RMS error becomes smaller after the swapping. \square

Remark. *Theorem 1 means that swapping two measurements that are not in order can reduce measurement noise. In other words, the noise can be minimized by placing all measurements in order.*

3.2. SOC and SOH estimation

Once the OCV during the relaxation is identified, the only missing piece in SOC and SOH estimation is estimating $\frac{dOCV}{dt}$. When the current is constant and when the capacitor in the ECM reaches a steady state, the terminal voltage can be calculated by:

$$U_{ter} = OCV + I(R_1 + R_2) \quad (13)$$

As a result, for the derivative of terminal voltage $\frac{dU_{ter}}{dt}$, we have:

$$\frac{dU_{ter}}{dt} = \frac{dOCV}{dt} + I \frac{dSOC}{dt} \left(\frac{dR_1}{dSOC} + \frac{dR_2}{dSOC} \right) \quad (14)$$

Both $\frac{dOCV}{dt}$ and $\frac{dSOC}{dt}$ are proportional to I . Therefore, when the current is small, we can neglect the final part in (14) since it is proportional to I^2 , and (14) becomes:

$$\frac{dU_{ter}}{dt} \approx \frac{dOCV}{dt} \quad (15)$$

(15) points out that $\frac{dU_{ter}}{dt}$, which can be easily calculated through linear regression, can be used to approximate $\frac{dOCV}{dt}$ when the current is low. One thing to note is that $\frac{dU_{ter}}{dt}$ is related to SOC. So, to ensure the SOC is the same as the SOC in parameter estimation, the voltage data right before the relaxation is used to do the regression analysis and determine $\frac{dU_{ter}}{dt}$ and $\frac{OCV}{dt}$.

Besides constant-current(CC) charging, our algorithm can also be implemented during constant-voltage (CV) charging. In this case, noticing that $\frac{dU_{ter}}{dt} = 0$, the derivative of (13) is

$$\frac{dOCV}{dt} + \frac{dI}{dt}(R_1 + R_2) + I \frac{dSOC}{dt} \left(\frac{dR_1}{dSOC} + \frac{dR_2}{dSOC} \right) = 0 \quad (16)$$

Since the current during the CV charging is usually small, we can neglect the final part in (16) since it is proportional to I^2 , and (16) becomes:

$$\frac{dOCV}{dt} + \frac{dI}{dt}(R_1 + R_2) \approx 0 \quad (17)$$

Since R_1 and R_2 can be estimated by using (10) and (12), the value of $\frac{dOCV}{dt}$ during the constant-voltage charge can be easily estimated by using (17).

Once $\frac{dOCV}{dt}$ and OCV are estimated, the SOC and SOH can be calculated by using (4) and (5). Namely, as shown in (18), the SOH is initially set to 100%, and (4) is used to solve the value of SOC. Next, the value of SOC is substituted into (5) to update the SOH. Afterward, the two processes described above are repeated until both estimations converge.

$$\begin{cases} SOH_0 = 1 \\ SOC_k = f^{-1}(OCV, SOH_k, T) \\ SOH_{k+1} = \frac{I}{Q_0} \frac{\partial OCV}{\partial SOC} \frac{dt}{dOCV} \end{cases} \quad (18)$$

A flow chart of the entire SOC and SOH estimation scheme is presented in Figure 3(a). Note that the SOC in the output is the cell's SOC in the first relaxation. Since SOC changes fast, another algorithm (such as coulomb counting) is usually needed to keep tracking the SOC afterward, and an example of such an algorithm will be detailed in Section 3.3. Generally, the proposed method only requires simple matrix operations and has no hyperparameter. The only special requirement for the charging profile is an extra two-minute relaxation during CC (or CV) charging.

However, when the current is high (above 0.5 C), the approximation in (15) would be no longer accurate since $I \frac{d(R_1+R_2)}{dt}$ will not be negligible. To address this problem, we proposed another variant of the SOC and SOH estimation method, which performs the parameter estimation a second time after the cell charges for a short while. While this will double the total relaxation time and calculation complexity, it can bring two benefits. First and foremost, by comparing the results from the first and second parameter estimation, we can know how much $(R_1 + R_2)$ has changed during that short period and calculate $d(R_1 + R_2)/dt$, which can help us better estimate $dOCV$. The second benefit is that the estimation result can be more accurate if the estimation is done twice and averaged. A flow chart of the entire SOC and SOH estimation scheme with this extra dR compensation is presented in Figure 3(b).

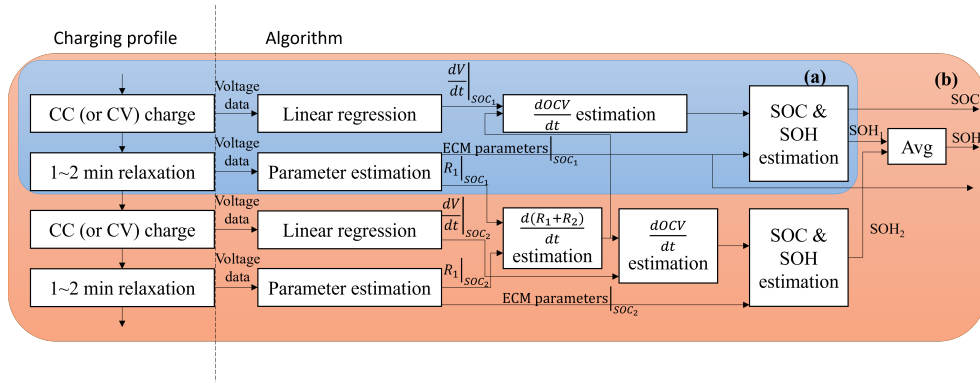


Figure 3: A flow chart of the proposed SOC and SOH estimation method: (a) without dR compensation (b) with dR compensation

3.3. SOC tracking method

The method shown in Figure 3 outputs the SOC and SOH during the first relaxation period. The method can be repeated after several cycles to keep track of the SOH. As for the SOC, however, it changes very quickly during operation. As a result, it is necessary to propose a method to keep tracking the SOC after the SOC and SOH of the cell during the relaxation are estimated. Note that the current is the same for all the cells connected in series in a battery pack. Therefore, according to (2), the SOC of different cells has the following correlation:

$$\Delta SOC_j = \Delta SOC_i \times \frac{SOH_i}{SOH_j} \quad (19)$$

where ΔSOC_i is the change of SOC of Cell i after the SOC and SOH estimation is done. According to (19), the SOC of each cell in the string can be calculated once the SOC of any single cell is estimated. Since the SOC tracking method here does not need to be repeated for every cell, it can be more complex, like a filter-based SOC estimation method.

In algorithm 1, an example of using an EKF for SOC tracking is provided. The method selects SOC and the capacitor voltage of Cell i (the reference cell) as the states of the system. Note that all the inputs of the algorithms come from the measurement data and the output of the SOC and SOH estimation algorithm presented in Figure 3.

It is worth noting that, in algorithm 1, all the parameters in the ECM are considered to be constants, which is actually not true in reality. Nevertheless,

Algorithm 1 SOC tracking algorithm based on extended Kalman filter

Inputs: $SOC_0, SOH, R_1, R_2, C, I_k, U_{ter,k}, Temp_k, t_k$
 $k = 0$
while the BMS is on **do**
 $k = k + 1$
 $\Delta t = t_k - t_{k-1}$

$$\begin{bmatrix} SOC_k(i) \\ U_{c,k} \end{bmatrix} = \begin{bmatrix} 1 & 0 \\ 0 & e^{-\Delta t/(R_2 C)} \end{bmatrix} \begin{bmatrix} SOC_{k-1}(i) \\ U_{c,k-1} \end{bmatrix} + \begin{bmatrix} \frac{\Delta t}{Q_0 SOH_i} \\ R_2(1 - e^{-\Delta t/(R_2 C)}) \end{bmatrix} I_k$$

$$P_k = \begin{bmatrix} 1 & 0 \\ 0 & e^{-2\Delta t/(R_2 C)} \end{bmatrix} P_{k-1} + Q_k$$

$$y_k = U_{ter,k} - OCV(SOC_k(i), SOH_i, Temp_k) - U_{c,k} - R_1 I_k$$

$$H_k = \begin{bmatrix} \frac{\partial OCV}{\partial SOC} \Big|_{SOC=SOC_k(i), Temp=Temp_k} & 1 \end{bmatrix}$$

$$S_k = H_k P_k H_k^T + R_k$$

$$K_k = P_k H_k^T S_k^{-1}$$

$$\begin{bmatrix} SOC_k(i) \\ U_{c,k} \end{bmatrix} = \begin{bmatrix} SOC_k(i) \\ U_{c,k} \end{bmatrix} + K_k y_k$$

$$P_k = (I - K_k H_k) P_k$$

for $j = 1$ to N **do**

$$SOC_k(j) = SOC_0(j) + (SOC_{i,k} - SOC_0(i)) \times \frac{SOH_i}{SOH_j}$$

end for
Output SOC_k
end while

where N is the total number of cells in the battery pack. i can be chosen arbitrarily. The algorithm inputs include the measured temperature, voltage, current, estimated SOC (during the relaxation), and estimated SOH of each cell. For Cell i (the reference cell), its estimated ECM parameters are also required as the inputs. The output is the SOC of each cell in the battery pack. R_k and Q_k are, respectively, the process noise covariance matrix and the measurement covariance matrix, and they can be determined based on the method presented in [35].

the algorithm can still yield a satisfactory result if the possible parameter changes are considered part of the measurement and process noise. Additionally, it is easy to prove that when the sampling frequency is high enough (in which case the linearization of the output function in each step can be considered perfect), all the states in the model are observable, and the convergence is therefore guaranteed. By contrast, suppose that a model parameter (such as the internal resistance) is instead considered to be a time-varying third state. In that case, the system's observability would depend on the input, and there may be no guarantee for convergence even if the sampling frequency is high enough. Therefore, only two states are included in the EKF.

4. Theoretical analysis

4.1. Sensitivity analysis

In section 3.1, when the three measurements y_1, y_2, y_3 are noisy, the estimation of the three ECM parameters R_2, C, OCV can also be inaccurate. When such noise is small, the correlation between the error of measurement and the error of parameter estimation can be found by taking the derivative of the (11), which is

$$\begin{bmatrix} \frac{dR_2}{R_2} \\ \frac{dC}{C} \\ \frac{dOCV}{OCV} \end{bmatrix} = \begin{bmatrix} \frac{x_3 e^{bx_3} - x_2 e^{bx_2}}{a(A_1 + A_2 - A_3)} & \frac{x_1 e^{bx_1} - x_3 e^{bx_3}}{a(A_1 + A_2 - A_3)} & \frac{x_2 e^{bx_2} - x_1 e^{bx_1}}{a(A_1 + A_2 - A_3)} \\ \frac{(bx_2 - 1)e^{bx_2} - (bx_3 - 1)e^{bx_3}}{ab(A_1 + A_2 - A_3)} & \frac{(bx_3 - 1)e^{bx_3} - (bx_1 - 1)e^{bx_1}}{ab(A_1 + A_2 - A_3)} & \frac{(bx_1 - 1)e^{bx_1} - (bx_2 - 1)e^{bx_2}}{ab(A_1 + A_2 - A_3)} \\ \frac{1}{OCV} \frac{A_2}{A_1 + A_2 - A_3} & \frac{1}{OCV} \frac{-A_3}{A_1 + A_2 - A_3} & \frac{1}{OCV} \frac{A_1}{A_1 + A_2 - A_3} \end{bmatrix} \begin{bmatrix} dy_1 \\ dy_2 \\ dy_3 \end{bmatrix} \quad (20)$$

where $a = R_2 I_0$, $b = -\frac{1}{R_2 C} < 0$, $A_1 = (x_2 - x_1)e^{\frac{x_3 - x_2}{R_2 C}}$, $A_2 = (x_3 - x_2)e^{\frac{x_1 - x_2}{R_2 C}}$, and $A_3 = x_3 - x_1$.

Since the three measurements are done using the same voltmeter, we can assume that the variance of the three measurements are the same and are all equal to σ_y^2 . In this case, the covariance of the estimation of the three parameters are

$$\sigma_{R_2}^2 = \frac{(x_3 e^{bx_3} - x_2 e^{bx_2})^2 + (x_1 e^{bx_1} - x_3 e^{bx_3})^2 + (x_2 e^{bx_2} - x_1 e^{bx_1})^2}{a^2(A_1 + A_2 - A_3)^2} R_2^2 \sigma_y^2 \quad (21)$$

$$\sigma_C^2 = \frac{(b_2 e^{bx_2} - b_3 e^{bx_3})^2 + (b_3 e^{bx_3} - b_1 e^{bx_1})^2 + (b_1 e^{bx_1} - b_2 e^{bx_2})^2}{a^2 b^2 (A_1 + A_2 - A_3)^2} C^2 \sigma_y^2 \quad (22)$$

$$\sigma_{OCV}^2 = \frac{A_1^2 + A_2^2 + A_3^2}{(A_1 + A_2 - A_3)^2} \sigma_y^2 \quad (23)$$

where $b_i = bx_i - 1, i = 1, 2, 3$.

Since the final purpose of parameter estimation is to estimate the SOC and SOH, and only OCV is directly related to the SOC and SOH, it is only necessary to minimize the covariance of OCV estimation. In other words, if we define $f(x_1, x_2, x_3) = \sigma_{OCV}^2/\sigma_y^2$, the objective function of the optimization problem can be formulated as $\min_{x_1, x_2, x_3} f$. The following theorems are introduced to solve this optimization problem.

Theorem 2. *When $x_3 - x_1 \rightarrow 0, f \rightarrow \infty$; when $x_3 - x_2 \rightarrow \infty, f \rightarrow 1$; when $x_2 - x_1 \rightarrow \infty, f \rightarrow \frac{1+e^{\frac{2(x_3-x_2)}{R_2C}}}{(e^{\frac{x_3-x_2}{R_2C}} - 1)^2}$.*

Proof. When $x_3 - x_1 \rightarrow 0$, both $x_2 - x_1$ and $x_3 - x_2$ also $\rightarrow 0$. So,

$$A_1 + A_2 - A_3 = o(x_d) \quad (24)$$

where $x_d = \max(x_2 - x_1, x_3 - x_2)$. While

$$A_1^2 + A_2^2 + A_3^2 = O(x_d^2) \quad (25)$$

So,

$$f = \frac{A_1^2 + A_2^2 + A_3^2}{(A_1 + A_2 - A_3)^2} = \frac{O(x_d^2)}{o(x_d^2)} \rightarrow \infty \quad (26)$$

On the other hand, when $x_3 - x_2 \rightarrow \infty, A_1 \gg A_3 \gg A_2$, so

$$f = \frac{A_1^2 + A_2^2 + A_3^2}{(A_1 + A_2 - A_3)^2} \approx \frac{A_1^2}{A_1^2} = 1 \quad (27)$$

Meanwhile, when $x_2 - x_1 \rightarrow \infty, A_1 = e^{\frac{x_3-x_2}{R_2C}} A_3 \gg A_2$, so

$$f = \frac{A_1^2 + A_2^2 + A_3^2}{(A_1 + A_2 - A_3)^2} \approx \frac{1 + e^{\frac{2(x_3-x_2)}{R_2C}}}{(e^{\frac{x_3-x_2}{R_2C}} - 1)^2} \quad (28)$$

□

Theorem 2 suggests that increasing the time interval between the second and third points can improve the algorithm's noise tolerance. However, when the time interval is larger, the required relaxation time for the cell will be longer, which would cause more delay in the charging process. As a result, it is necessary to optimize the position of x_2 when the total time interval is constrained. To address this issue, we have the following theorem.

Theorem 3. When x_1 and x_3 are fixed, and $x_3 - x_1 \ll R_2C$, the minimum of $\sigma_{OCV}^2/\sigma_y^2$ is obtained when $x_2 = \frac{x_1+x_3}{2}$.

Proof. When $x_3 - x_1 \ll R_2C$, $x_3 - x_2$ and $x_2 - x_1$ are also $\ll R_2C$, so

$$\frac{\partial A_1}{\partial x_2} = 1 - 2kx_2 + kx_1 + kx_3 + o(x_3 - x_1) \quad (29)$$

$$\frac{\partial A_2}{\partial x_2} = -1 + 2kx_2 - kx_1 - kx_3 + o(x_3 - x_1) \quad (30)$$

$$\frac{\partial A_3}{\partial x_2} = 0 \quad (31)$$

As a result, $\frac{\partial A_1}{\partial x_2} + \frac{\partial A_2}{\partial x_2} = o(x_3 - x_1)$. When f is minimized, $\frac{\partial f}{\partial x_2} = 0$, so

$$(2A_1 \frac{\partial A_1}{\partial x_2} + 2A_2 \frac{\partial A_1}{\partial x_2})(A_1 + A_2 - A_3) - 2(A_1^2 + A_2^2 + A_3^2)(\frac{\partial A_1}{\partial x_2} + \frac{\partial A_2}{\partial x_2}) = 0 \quad (32)$$

Substituting (29) and (30) into (32), we have:

$$\frac{\partial A_1}{\partial x_2}(A_1 - A_2)(A_1 + A_2 - A_3) = o((x_3 - x_1)^3) \quad (33)$$

If $\frac{2x_2}{x_1+x_3} \neq 1$, then $\frac{\partial A_1}{\partial x_2} = O(1)$, $A_1 - A_2 = O(x_3 - x_1)$, $A_1 + A_2 - A_3 = O(x_3 - x_1)$, and (33) cannot be satisfied. As a result, when $\frac{\partial f}{\partial x_2} = 0$, $\frac{2x_2}{x_1+x_3} = 1$ must be satisfied. Noticing that this is the only point where $\frac{\partial f}{\partial x_2} = 0$, f must either reach maximum or minimum. Since when $x_2 = x_1$ or when $x_2 = x_3$, $f = +\infty$, we can conclude that f is minimized at $x_2 = \frac{x_1+x_3}{2}$ when $x_3 - x_1$ is small. \square

While theorem 3 suggests that the optimal selection of x_2 is $\frac{x_1+x_3}{2}$, such a conclusion is based on the assumption that x_3 is small. To study if choosing $x_2 = \frac{x_1+x_3}{2}$ is still reasonable when x_3 is large, in Figure 4, a comparison of the noise amplification rate is made between the two x_2 selection schemes. The first scheme is to optimize x_2 so that the noise amplification rate is the lowest, while the second scheme is to select x_2 as $\frac{x_1+x_3}{2}$. It can be seen that the two curves always have little difference, meaning that selecting x_2 as $\frac{x_1+x_3}{2}$ can always give a good result.

In fact, selecting $x_2 = \frac{x_1+x_3}{2}$ also has another benefit: the function set (11) can have a closed-form solution and can be directly calculated by using

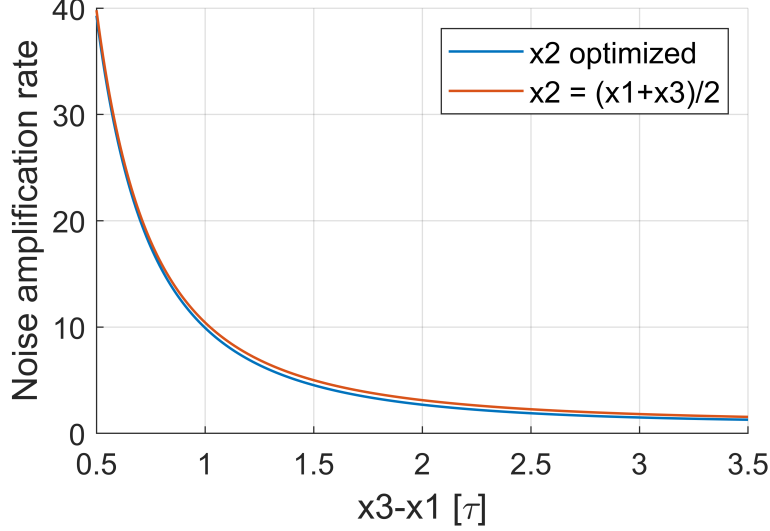


Figure 4: The noise amplification rate at different x_3 (when $x_1 = 0$), $\tau = R_2C$

(12). Meanwhile, if x_2 is chosen arbitrarily, the parameter needs to be calculated using algorithms like gradient descent, which damages the algorithm's simplicity. Considering all the above, x_2 is selected as $\frac{x_1+x_3}{2}$ in this paper.

Finally, it is necessary to study how f changes as x_1 and x_3 change. Regarding this, we provide the following theorem.

Theorem 4. *When $x_2 = \frac{x_1+x_3}{2}$, a larger x_3 or a smaller x_1 can make f smaller.*

Proof. If we define $x_d = x_3 - x_2 = x_2 - x_1$, f would only be related to x_d , and the theorem we are trying to prove becomes equivalent to $\frac{df}{dx_d} < 0$. And we have

$$A_1 = x_d e^{\frac{x_d}{R_2C}}, A_2 = x_d e^{-\frac{x_d}{R_2C}}, A_3 = 2x_d \quad (34)$$

Therefore, if we define $m = e^{\frac{x_d}{R_2C}} > 1$, we have

$$\begin{aligned} f &= \frac{A_1^2 + A_2^2 + A_3^2}{(A_1 + A_2 - A_3)^2} \\ &= \frac{m^2 + m^{-2} + 4}{(m + m^{-1} - 2)^2} \\ &= \frac{m^4 + 4m^2 + 1}{(m - 1)^4} \end{aligned}$$

Consequently,

$$\frac{df}{dm} = \frac{-8m^3 - 16m - 4}{(m - 1)^5} < 0 \quad (35)$$

Since $\frac{dm}{dx_d} > 0$, it can be concluded that $\frac{df}{dx_d} < 0$, which means that a larger x_3 or a smaller x_1 can make f smaller. \square

4.2. Convergence analysis

In (18), an iterative method was proposed for SOC and SOH estimation. While the method can theoretically be applied at any time during the charging process, the estimation accuracy varies due to several factors. One of the most important ones is the convergence of the method. Since the OCV curve is a nonlinear function of SOC and SOH (for a constant temperature), the iterative process can converge more quickly in a specific SOC range. Therefore, to improve the estimation accuracy, it is necessary to analyze the convergence of the method and pick the best time to use it.

Suppose that the true SOC and SOH are respectively SOC_{true} and SOH_{true} , according to (18),

$$SOH_{true} = \frac{I}{Q_0} \frac{dt}{dOCV} \left. \frac{\partial OCV}{\partial SOC} \right|_{SOC_{true}, SOH_{true}} \quad (36)$$

The iteration process in (18) can therefore be written as

$$SOH_{k+1} = g(SOH_k) = \frac{SOH_{true} \left. \frac{\partial OCV}{\partial SOC} \right|_{SOC_k, SOH_k}}{\left. \frac{\partial OCV}{\partial SOC} \right|_{SOC_{true}, SOH_{true}}} \quad (37)$$

We define the iteration to be locally convergent at $A = (SOC_{true}, SOH_{true})$ when there exists a neighborhood of A , and the iterative method will converge to A when the initial point is in the neighborhood. Suppose that the derivative of SOC_k and $\frac{dOCV}{dSOC}$ to SOH_k are continuous in the domain, then the local convergence of the method can be judged by the derivative of g , which is defined in (38).

$$L = \left. \frac{dg}{dSOH} \right|_{SOC_{true}, SOH_{true}} = SOH_{true} \left. \frac{\frac{\partial^2 OCV}{\partial SOC^2} \frac{\partial SOC}{\partial SOH} + \frac{\partial^2 OCV}{\partial SOC \partial SOH}}{\frac{\partial OCV}{\partial SOC}} \right|_{SOC_{true}, SOH_{true}} \quad (38)$$

where

$$\left. \frac{\partial SOC}{\partial SOH} \right|_{SOH_{true}, SOC_{true}} = \left. \frac{\partial f^{-1}(OCV, SOH, T)}{\partial SOH} \right|_{SOH_{true}, SOC_{true}} \quad (39)$$

When $|L| < 1$, we can prove that the iteration is locally convergent, since $\frac{|SOH_{k+1}-SOH_{true}|}{|SOH_k-SOH_{true}|} < |L| + \epsilon < 1$. On the other hand, when $L > 1$, the method will not converge locally because in the neighborhood, $\frac{|SOH_{k+1}-SOH_{true}|}{|SOH_k-SOH_{true}|} > |L| - \epsilon > 1$, and SOH_k will finally move out of the neighborhood. The value of $|L|$ as a function of SOC_{true} and SOH_{true} is shown in Figure 5. In the figure, for better visualization, all the areas where $|L| > 1$ are rescaled to $|L| = 1$, and other areas represent the domain where the method is locally convergent.

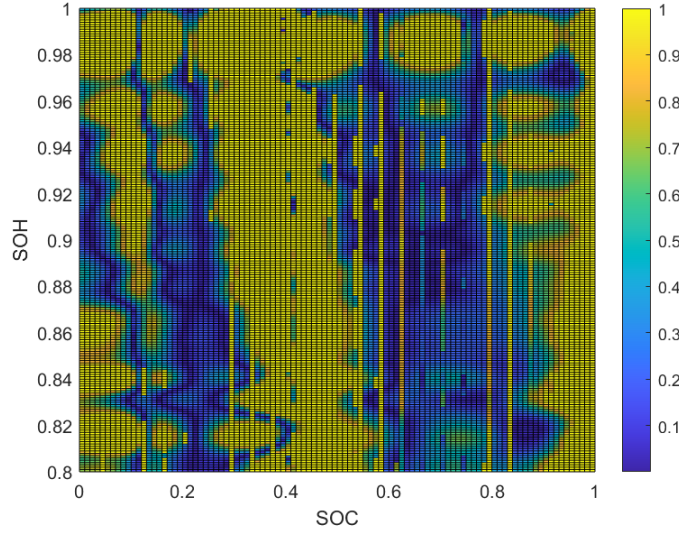


Figure 5: Local convergence analysis

The local convergence analysis can tell us what outputs are possible and what are not. For example, if the iterative method is used at 50% SOC , it will almost always give inaccurate results since it hardly ever converges at 50% SOC , regardless of the true SOH . However, local convergence analysis alone is not enough to evaluate the estimation error since local convergence doesn't guarantee global convergence, and not converging at a certain point doesn't necessarily mean a high estimation error. To better evaluate the accuracy limit of the iterative method, another simulation was performed to analyze the correlation between SOC_{true} and estimation accuracy. Namely, for each SOC_{true} between 0% to 100%, we enumerate the values of SOH_{true} from 80% to 100% and calculate the average estimation error (measured by

root mean square error, or RMSE) when the iterative method is initialized at $SOH_0 = 100\%$. The results are shown in Figure 6.

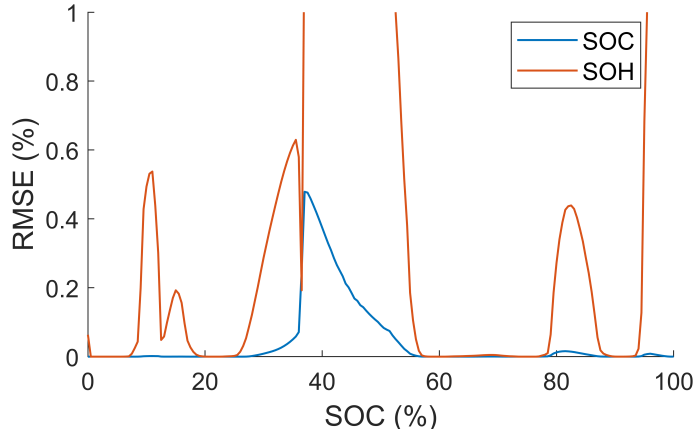


Figure 6: Iteration error analysis

According to Figure 6, the accuracy of SOC estimation is always relatively high, as the maximum RMSE of SOC is only 0.5%. In contrast, the accuracy of SOH estimation varies more significantly to the SOC_{true} when using the method. Since the error of SOC estimation can be higher in practice, the best timing to use our method is between 57% and 77% SOC, where both errors are very close to zero, meaning that the method can always converge to the correct values.

5. Experimental validation

5.1. Experimental validation setup

Six lithium-ion batteries of NMC chemistry (model ICR18650-22F) manufactured by SAMSUNG were placed inside six separate temperature control chambers and were used for experimental validation. The charging and discharging were monitored by the battery tester manufactured by Arbin Instruments. Data collection and the setup of charging and discharging profiles were done using the supporting software Mits Pro. The RMSEs of the voltage and current measurements are 0.15 mV and 0.1 mA, respectively. The testing profile for each cell was precisely the same and is shown in Figure 7.

As is shown in Figure 7, the cells were aged at 40°C by running continuous 1 C charge and 2 C discharge until the SOH dropped below 75%. A

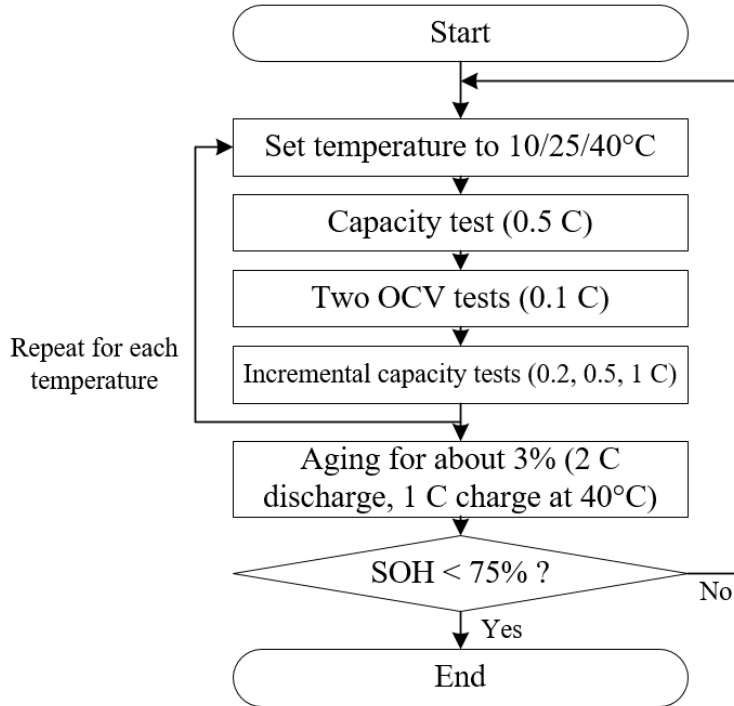


Figure 7: A flow chart of the aging test

set of characteristic tests was performed for each cell at at least nine different aging levels. Each characteristic test consisted of a capacity test (to stabilize the cell temperature), two OCV tests (incremental OCV test and low-current OCV test), and three incremental capacity tests at different C rates. All these characteristic tests were repeated at three different temperatures. The meanings of the two OCV tests have already been illustrated in section 2.2. The charge and discharge rates used in the low-current OCV test and incremental OCV test were both 0.1 C. The relaxation time in the incremental OCV test was 3 minutes, much shorter than the typical setup. The purpose of shortening the relaxation time is to make the OCV in the OCV experiment more consistent with the OCV identified from the battery ECM and, hence, to improve the SOC and SOH estimation accuracy. In the incremental capacity tests, the cells were fully charged and discharged at a constant current until the SOC dropped by 3%. Afterward, the cell rested for three minutes, followed by a 10-second 1 C discharge and another 3-minute rest. Then, the cell was discharged again, and the procedures de-

scribed above were repeated until the cell was fully discharged. The cell then rested for 30 minutes and was charged using a constant current constant voltage profile afterward. Likewise, whenever the SOC rose by 5%, the cell rested for 3 minutes, was discharged for 10 seconds, and rested for another 3 minutes until the cell was fully charged. The purpose of such a charging and discharging profile was to enable the validation of our parameter estimation algorithm at the most desirable SOC.

According to the conclusions in Section 4.2, the best time to use the method is when the actual SOC is between 55% and 77%. However, in practice, the SOC is unknown before the state estimation, so the SOC is not a good indicator of when to use the method. Under this consideration, we used the terminal voltage as the indicator during validation instead. Namely, among more than twenty relaxations during the charging process in the incremental capacity test, the method is used when the terminal voltage at the beginning of the relaxation exceeds 3.9 V. This voltage threshold can guarantee that the SOC during this and the following relaxation are both between 55% and 77%, regardless of the SOH and the C rate.

According to theorem 4 and 3 in section 4.1, when estimating the ECM parameters, the optimal selection of the three points should be $x_1 = 0, x_2 = x_3/2$, and $50s \leq x_3 \leq 120s$ (depending on the estimation accuracy). However, theorem 4 is based on the assumption that the ECM precisely describes the dynamic voltage response of the battery, which is, in fact, not true. In practice, it is found that the ECM model can only approximate the cell's voltage response between 10s to 300s well. As a result, we instead selected $x_1=10s, x_2 = \frac{x_1+x_3}{2}$, and $60s \leq x_3 \leq 180s$.

During the experimental validation, the OCV curve was fitted based on the voltage data in the incremental OCV test. Since the proposed SOC and SOH estimation method is used during the charging process, we only used the charge OCV data to fit the OCV curve, as the charge OCV curve is slightly different from the discharge OCV curve. After fitting the OCV curve, we validated our method on the experimental data in the three incremental capacity tests. Such a process was repeated at each temperature. As previously mentioned, when validating on a particular cell, the OCV data of this cell was excluded when fitting the OCV curve. For example, when estimating the SOC and SOH of Cell 3, the OCV curve we used was fitted on the data of Cells 1, 2, 4, 5, and 6. The reason for such an arrangement was to separate the fitting data and validation data.

5.2. Experimental results

When $x_3 = 120\text{s}$, our method's SOC and SOH estimation results with and without dR compensation are shown in Figure 8. The average run time of these two variants is, respectively, 0.33 ms and 0.51 ms.

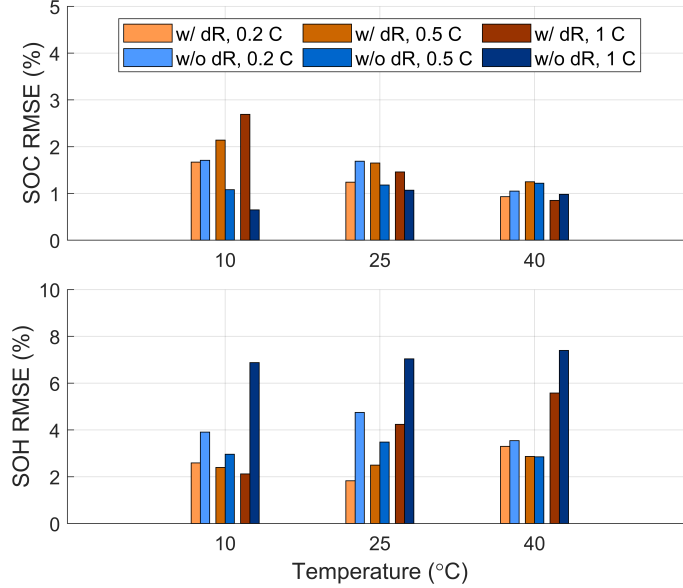


Figure 8: SOC and SOH estimation errors of our method with and without dR compensation (two-minute relaxation time)

According to the figure, the proposed method can realize fast and accurate SOC and SOH estimation under various temperatures and C rates. When the C rate is equal to or lower than 0.5 C, the variant without dR compensation is enough for accurate estimation, with a SOC and SOH error of about 2% and 3.5%. Note that this variant only requires a relaxation of two minutes and a computational time of 0.33 ms. If the charging current is higher than 0.5 C or the requirement for estimation accuracy is higher, then using the variant with dR compensation would be better. While this other variant is more complex, it still only needs a four-minute relaxation time and a computational time of 0.51 ms. This means that even if this variant is applied to an EV with 8,000 cells, the total computational time would still be lower than five seconds.

To verify the method's sensitivity to the relaxation time (x_3), in Figure 9, the average SOC and SOH estimation error at different relaxation time and temperatures are plotted. The results show that the estimation error

is not very sensitive to the relaxation time after it exceeds 60 seconds. The lowest error is achieved at $x_3 = 120$ s, suggesting that relaxing the cells for more than two minutes is unnecessary.

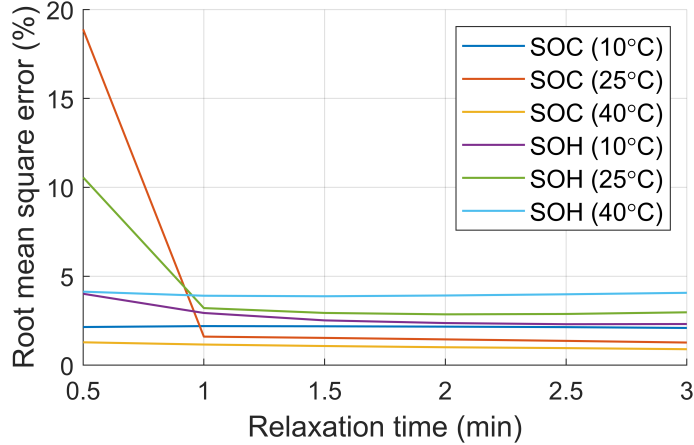


Figure 9: Selection of the relaxation time (x_3)

5.3. Comparison against Unscented Kalman Filter

Compared with other model-based methods (for example, EKF and UKF), the method proposed in this paper has significantly less computational complexity and needs no hyperparameter or initialization. However, it requires the cell to rest for one to four minutes during the charging process, while other model-based methods do not have such requirements. As a result, to better evaluate the pros and cons of the proposed method, it is necessary to make a quantitative comparison with other model-based methods in terms of their accuracy and computational complexity.

In this paper, the UKF algorithm was chosen as the baseline algorithm. While another KF-based method was used in Section 3.3 for SOC tracking, the purpose differed. In Section 3.3, EKF was only used to estimate the SOC of one cell for each battery string, under which circumstance all the states of the model are observable, and the convergence is guaranteed; but here, the UKF is used to estimate the SOC and SOH of each cell in the pack, and not the states are not always fully observable.

The UKF used in this paper has three states: remaining capacity Q_r , capacitor voltage U_c , and present maximum capacity Q . With these definitions, the discrete state-space representation of the system can be written as (40).

The correlation between these states and the SOC and SOH is formulated in (1) and (3). We didn't directly define *SOC* and *SOH* as the states to make the state transition functions linear.

$$\begin{cases} \begin{bmatrix} Q_{r,k} \\ U_{c,k} \\ Q_k \end{bmatrix} = F \begin{bmatrix} Q_{r,k-1} \\ U_{c,k-1} \\ Q_{k-1} \end{bmatrix} + BI_k \\ U_{ter,k} = f_{OCV}(\frac{Q_{r,k}}{Q_k}, \frac{Q_k}{Q_0}) + U_{c,k} + R_1 I_k \end{cases} \quad (40)$$

$$F = \begin{bmatrix} 1 & 0 & 0 \\ 0 & e^{-\frac{\Delta t}{R_2 C}} & 0 \\ 0 & 0 & 1 \end{bmatrix}, B = \begin{bmatrix} \Delta t \\ R_2 - R_2 e^{-\frac{\Delta t}{R_2 C}} \\ 0 \end{bmatrix} \quad (41)$$

where Δt is the time interval between two steps, and B and F are two constant matrices defined by (41).

The UKF was validated on the same data as our method (with *dR* compensation) for a fair comparison. Specifically, the profile includes a three-minute relaxation, a 10-second 1 C discharge pulse, another 3-minute relaxation, a constant-current charging that increases the SOC by 5%, and another 3-minute relaxation. During the first relaxation, the UKF was not turned on, and the voltage data was used to estimate the values of all the ECM parameters. The parameter estimation method is the same as in Section 3.1. Starting from the discharge pulse, the UKF was turned on, with the initial SOH estimation set to 100%, the initial capacitor voltage set to 0, and the initial SOC set to be the inverse of the OCV during the first relaxation. The SOC and SOH estimation at the very end of the profile are considered estimation outputs and compared against the actual value to calculate the error. The detailed hyperparameter setup for this UKF is the same as in [35].

The SOC and SOH estimation results by using UKF are presented in Figure 10. The figure suggests that our method is hundreds of times faster than the UKF and is more accurate, especially for SOC estimation.

5.4. Error analysis

While the SOC and SOH estimation error of the proposed method is relatively low, it is still essential to understand the source of the error, as understanding the error sources can help us better analyze the applicability and the pros and cons of the method. For this purpose, the validation was

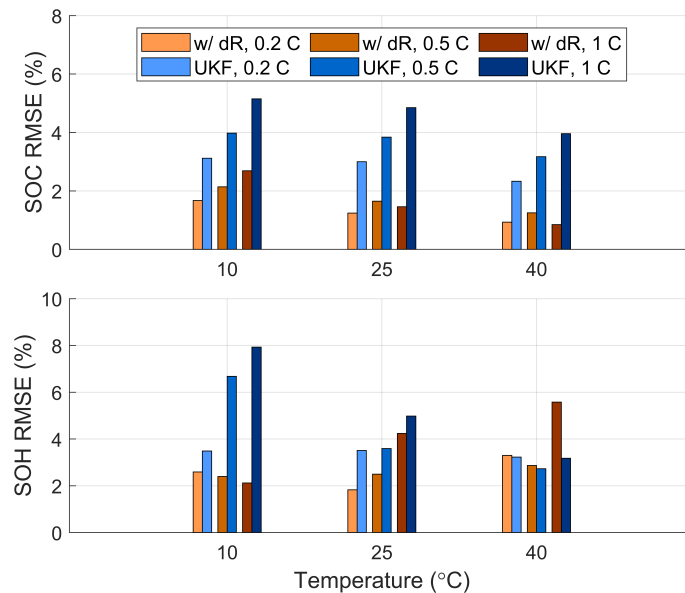


Figure 10: Comparison between our method (average run time = 0.51 ms) and UKF (average run time = 73 ms)

done another eighteen times, each time on a different setup. As is shown in the first column of Table 5.4, these extra validations can be separated into three groups according to the data source used in the validation. In the first group, all the validations were done on experimental data. In the second and third groups, only the current data were from the experiment, and all the voltage data came from a simulated battery model. The difference is that the battery model used in the second group is a second-order RC model, while the one used in the third group is a first-order RC model. In other words, only the model used in the third group is the same as the battery model we used when proposing the method. By default, when generating the voltage data, it is assumed that there is a voltage noise with a standard deviation of 0.15 mV (the same as the standard deviation of the voltmeter in the experiment), and all the RC parameters change as the SOC changes.

We started with the default setting for each data source and gradually added more simplifications. For example, in the fourth scenario, we not only used the simplification “Known SOC” but also applied the simplification “More relevant data” and “Fixed OCV curve”. In other words, in Table 5.4, within each group, the difficulty of the estimation becomes gradually lower

from top to bottom. Specifically, for experimental data, “More relevant data” means that the OCV curve we used came from the same cell that we were validating on (note that by default, the OCV curve came from the data of all the other cells besides the cell that we were validating on); “Fixed OCV curve” means that we stopped updating the OCV curve as we updated the SOH estimation, and always used the OCV curve corresponding to the true SOH; “Known SOC” means that we assume that we used the actual SOC instead of the estimated SOC when estimating the SOH. For simulation data, “Known capacitor voltage” means that the actual value of the capacitor voltage before entering the relaxation, which was previously assumed to be R_2I , is known; “No voltage noise” means that the measurement voltage noise is set to zero, “Fixed RC parameter” means that the RC parameters in the simulation become constants instead of variables that change as SOC changes; “More accurate dV/dt” means that fewer points (two points instead of fifty points) are used in the linear regression to fit dV/dt. The meaning of “Fixed OCV curve” and “Known SOC” for simulation data are the same as for experimental data.

Among all the scenarios in Table 5.4, the most unique one is “Coulomb Counting”. For this setup, we didn’t use our SOC and SOH estimation method; instead, we used Coulomb Counting. As previously mentioned, the “true” SOC and “true” SOH are also calculated based on Coulomb Counting in the experimental validation. The difference is that our definition of SOH is the cell’s normalized charge capacity in the 0.1 C incremental OCV test. Yet, here, the SOH was estimated by the normalized charge capacity in the corresponding incremental capacity test, in which the charge current is not 0.1 C. For example, when the charge current is 0.1 C, the initial capacity of Cell 1 is 2.156 Ah, which decreases to 1.775 Ah after 900 cycles, resulting in an SOH of 82.3%. Meanwhile, when the maximum charge current is 1 C, the initial capacity of Cell 1 is 2.079 Ah, which decreases to 1.627 Ah after 900 cycles, resulting in an SOH of 78.3%. Such a 4% difference in SOH suggests that SOH is not a definite state of the battery, and its value can change under different conditions. The RMSE of the SOH estimation is used to quantify this uncertainty originating from the definition of SOH itself. Likewise, when we calculate the SOC based on the charge and discharge capacity calculated from the 0.1 C OCV test, the SOC at the end of the charging may not be precisely 100% since the cell’s capacity varies slightly at different C rates. The RMSE of the SOC estimation is calculated from the difference between the final calculated SOC and 100% and is used to

quantify the uncertainty originating from the definition of SOC. In essence, the error of Coulomb Counting can be considered the lower limit of the SOC and SOH estimation error when using experimental data since such an error comes from the definition of SOC and SOH and is impossible to avoid.

The SOC and SOH estimation errors in all these extra validations are presented in Table 5.4. Note that all the validations here were based on the data gathered at 25 °C, and we always added dR compensation when doing the estimation.

Table 1: RMSE of SOC and SOH estimation under different scenarios

Data Source	Scenarios	0.2 C		0.5 C		1 C	
		SOC	SOH	SOC	SOH	SOC	SOH
Experimental Data	Default	1.24%	1.83%	1.65%	2.50%	1.46%	4.24%
	More relevant data	1.24%	1.84%	1.69%	2.55%	1.57%	4.23%
	Fixed OCV curve	0.62%	2.31%	1.35%	2.84%	1.88%	4.44%
	Known SOC	0.62%	2.33%	1.35%	2.79%	1.88%	4.85%
	Coulomb Counting	0.20%	0.68%	0.77%	1.79%	0.38%	2.06%
2RC Model Simulation	Default	0.78%	2.92%	0.89%	7.50%	1.40%	11.72%
	Known capacitor voltage	1.29%	2.27%	2.37%	4.18%	3.70%	6.89%
	No voltage noise	1.14%	1.71%	2.55%	3.88%	3.74%	6.94%
	Fixed RC parameters	0.35%	0.52%	1.15%	0.81%	3.14%	3.39%
	More accurate dV/dt	0.35%	0.52%	1.14%	0.77%	3.12%	3.32%
	Fixed OCV curve	0.31%	0.14%	0.93%	0.42%	2.22%	2.39%
	Known SOC	0.31%	0.08%	0.93%	0.09%	2.22%	0.20%
1RC Model Simulation	Default	0.72%	2.57%	1.24%	6.11%	2.12%	11.41%
	Known Capacitor Voltage	1.05%	2.40%	1.44%	2.44%	1.26%	4.28%
	No voltage noise	0.85%	1.13%	1.40%	1.80%	1.20%	3.93%
	Fixed RC parameters	0.10%	0.50%	0.16%	0.62%	0.53%	1.25%
	More accurate dV/dt	0.11%	0.51%	0.17%	0.62%	0.47%	1.10%
	Fixed OCV curve	0.00%	0.00%	0.00%	0.00%	0.00%	0.00%
	Known SOC	0.00%	0.00%	0.00%	0.00%	0.00%	0.00%

Interestingly, when using our method on experimental data, no simplification can effectively improve the accuracy of the SOH estimated by our method, and only the “Fixed OCV curve” can marginally improve the accuracy of the SOC estimated by our method. Such a phenomenon suggests that all the error sources we examined in the first validation group are unimportant. According to the results in the second and third groups of validations, the critical error sources of our method are (1) our assumption that the capacitor has been fully charged before the start of the relaxation and (2) our linear approximation of $R_1(SOC)$ and $R_2(SOC)$. The second error source is very hard to avoid since estimating R_1 and R_2 in real-time is very hard. Yet, the first error source can be mitigated by prolonging the constant-current charging time before the relaxation. In the experiment, the length of constant-current charging is set to the time required to increase the SOC by

5%. Therefore, when the charge C rate is 1 C, the constant-current charging time is just 3 minutes, which is insufficient for the capacitor to charge fully. Such a difference in the length of constant-current charging explains why this error source affects higher C rates more than lower C rates. The estimation accuracy is expected to increase if we prolong the constant-current charging time.

Additionally, by comparing the corresponding scenarios in the second and third data sources, we can see that the estimation accuracy for these two data sources is, in fact, quite similar, even though the first-order RC model used in the parameter estimation only matches the third data source well. Such an observation suggests that although a more complex battery model can better simulate the voltage data, the simple first-order RC model will not necessarily lead to a higher SOC and SOH estimation error. Other error sources can dilute the benefit of a more complex model, and identifying more parameters also leads to weaker observability and longer computational time.

6. Conclusions

In this paper, an online battery SOC and SOH estimation method was proposed. The method is based on rigorous theoretical analysis and requires no hyperparameter fine-tuning. The method has two variants. The first variant is designed for low C-rate (≤ 0.5 C) charging and only requires a 1 to 2-minute relaxation, while the second can be used for higher C rates but requires a 2 to 4-minute relaxation during the charging process. Both variants can accurately estimate SOC and SOH at different temperatures. Specifically, the average computational time of the first variant is 0.33 ms, and the estimation RMSE for SOC and SOH are respectively around 1.2% and 4.8%. In comparison, the average computational time of the second variant is 0.51 ms, and the estimation RMSE for SOC and SOH are respectively around 1.5% and 3%. Compared with UKF, our method requires significantly lower computational time and has higher accuracy.

The main limitations of the work are that the proposed method requires a few minutes of relaxation at some specific SOC range (between 55% and 77%) and that the charging current cannot be too high (> 1 C) for accurate state estimation. Future work will focus on extending the method to a broader SOC range and fast-charging scenarios.

References

- [1] X. Hu, C. Zou, C. Zhang, Y. Li, Technological developments in batteries: a survey of principal roles, types, and management needs, *IEEE Power and Energy Magazine* 15 (5) (2017) 20–31.
- [2] J. Hou, T. Li, F. Zhou, D. Zhao, Y. Zhong, L. Yao, L. Zeng, A review of critical state joint estimation methods of lithium-ion batteries in electric vehicles, *World Electric Vehicle Journal* 13 (9) (2022) 159.
- [3] Y. Li, K. Liu, A. M. Foley, A. Zülke, M. Berecibar, E. Nanini-Maury, J. Van Mierlo, H. E. Hoster, Data-driven health estimation and lifetime prediction of lithium-ion batteries: A review, *Renewable and sustainable energy reviews* 113 (2019) 109254.
- [4] L. Ungurean, G. Cârstoiu, M. V. Micea, V. Groza, Battery state of health estimation: a structured review of models, methods and commercial devices, *International Journal of Energy Research* 41 (2) (2017) 151–181.
- [5] S. Jiang, Z. Song, A review on the state of health estimation methods of lead-acid batteries, *Journal of Power Sources* 517 (2022) 230710.
- [6] S. Zhang, X. Guo, X. Dou, X. Zhang, A rapid online calculation method for state of health of lithium-ion battery based on coulomb counting method and differential voltage analysis, *Journal of Power Sources* 479 (2020) 228740.
- [7] M. Berecibar, M. Garmendia, I. Gandiaga, J. Crego, I. Villarreal, State of health estimation algorithm of lifepo4 battery packs based on differential voltage curves for battery management system application, *Energy* 103 (2016) 784–796.
- [8] L. Zheng, J. Zhu, D. D.-C. Lu, G. Wang, T. He, Incremental capacity analysis and differential voltage analysis based state of charge and capacity estimation for lithium-ion batteries, *Energy* 150 (2018) 759–769.
- [9] S. Yang, C. Zhang, J. Jiang, W. Zhang, L. Zhang, Y. Wang, Review on state-of-health of lithium-ion batteries: Characterizations, estimations and applications, *Journal of Cleaner Production* 314 (2021) 128015.

- [10] R. Xiong, L. Li, J. Tian, Towards a smarter battery management system: A critical review on battery state of health monitoring methods, *Journal of Power Sources* 405 (2018) 18–29.
- [11] A. Manoharan, K. Begam, V. R. Aparow, D. Sooriamoorthy, Artificial neural networks, gradient boosting and support vector machines for electric vehicle battery state estimation: A review, *Journal of Energy Storage* 55 (2022) 105384.
- [12] J. Shi, D. Kato, S. Jiang, C. Dangwal, S. Moura, Robust estimation of state of charge in lithium iron phosphate cells enabled by online parameter estimation and deep neural networks, *IFAC-PapersOnLine* 56 (3) (2023) 127–132.
- [13] X. Shu, G. Li, J. Shen, Z. Lei, Z. Chen, Y. Liu, An adaptive multi-state estimation algorithm for lithium-ion batteries incorporating temperature compensation, *Energy* 207 (2020) 118262.
- [14] P. Shen, M. Ouyang, L. Lu, J. Li, X. Feng, The co-estimation of state of charge, state of health, and state of function for lithium-ion batteries in electric vehicles, *IEEE Transactions on vehicular technology* 67 (1) (2017) 92–103.
- [15] C. Yang, X. Wang, Q. Fang, H. Dai, Y. Cao, X. Wei, An online soc and capacity estimation method for aged lithium-ion battery pack considering cell inconsistency, *Journal of Energy Storage* 29 (2020) 101250.
- [16] S. Park, J. Ahn, T. Kang, S. Park, Y. Kim, I. Cho, J. Kim, Review of state-of-the-art battery state estimation technologies for battery management systems of stationary energy storage systems, *Journal of Power Electronics* 20 (6) (2020) 1526–1540.
- [17] Y. Xing, W. He, M. Pecht, K. L. Tsui, State of charge estimation of lithium-ion batteries using the open-circuit voltage at various ambient temperatures, *Applied Energy* 113 (2014) 106–115.
- [18] R. Zhang, B. Xia, B. Li, L. Cao, Y. Lai, W. Zheng, H. Wang, W. Wang, M. Wang, A study on the open circuit voltage and state of charge characterization of high capacity lithium-ion battery under different temperature, *Energies* 11 (9) (2018) 2408.

- [19] S.-L. Wang, X. Xiong, C.-Y. Zou, L. Chen, C. Jiang, Y.-X. Xie, D.-I. Stroe, An improved coulomb counting method based on dual open-circuit voltage and real-time evaluation of battery dischargeable capacity considering temperature and battery aging, *International Journal of Energy Research* 45 (12) (2021) 17609–17621.
- [20] L. Lavigne, J. Sabatier, J. M. Francisco, F. Guillemard, A. Noury, Lithium-ion open circuit voltage (ocv) curve modelling and its ageing adjustment, *Journal of Power Sources* 324 (2016) 694–703.
- [21] C. R. Birkl, M. R. Roberts, E. McTurk, P. G. Bruce, D. A. Howey, Degradation diagnostics for lithium ion cells, *Journal of Power Sources* 341 (2017) 373–386.
- [22] C. Weng, J. Sun, H. Peng, A unified open-circuit-voltage model of lithium-ion batteries for state-of-charge estimation and state-of-health monitoring, *Journal of power Sources* 258 (2014) 228–237.
- [23] S. Tong, M. P. Klein, J. W. Park, On-line optimization of battery open circuit voltage for improved state-of-charge and state-of-health estimation, *Journal of Power Sources* 293 (2015) 416–428.
- [24] Z. Ma, R. Yang, Z. Wang, A novel data-model fusion state-of-health estimation approach for lithium-ion batteries, *Applied energy* 237 (2019) 836–847.
- [25] D. Natella, S. Onori, F. Vasca, A co-estimation framework for state of charge and parameters of lithium-ion battery with robustness to aging and usage conditions, *IEEE Transactions on Industrial Electronics* 70 (6) (2022) 5760–5770.
- [26] M. Naguib, P. Kollmeyer, A. Emadi, Lithium-ion battery pack robust state of charge estimation, cell inconsistency, and balancing, *IEEE Access* 9 (2021) 50570–50582.
- [27] Z. Zhou, B. Duan, Y. Kang, N. Cui, Y. Shang, C. Zhang, A low-complexity state of charge estimation method for series-connected lithium-ion battery pack used in electric vehicles, *Journal of Power Sources* 441 (2019) 226972.

- [28] D. Huang, Z. Chen, C. Zheng, H. Li, A model-based state-of-charge estimation method for series-connected lithium-ion battery pack considering fast-varying cell temperature, *Energy* 185 (2019) 847–861.
- [29] J. Wei, G. Dong, Z. Chen, Y. Kang, System state estimation and optimal energy control framework for multicell lithium-ion battery system, *Applied Energy* 187 (2017) 37–49.
- [30] P. Gill, D. Zhang, L. D. Couto, C. Dangwal, S. Benjamin, W. Zeng, S. Moura, State-of-health estimation pipeline for li-ion battery packs with heterogeneous cells, in: *2022 American Control Conference (ACC)*, IEEE, 2022, pp. 1080–1086.
- [31] G. L. Plett, Extended kalman filtering for battery management systems of lipb-based hev battery packs: Part 3. state and parameter estimation, *Journal of Power sources* 134 (2) (2004) 277–292.
- [32] Q.-Q. Yu, R. Xiong, L.-Y. Wang, C. Lin, A comparative study on open circuit voltage models for lithium-ion batteries, *Chinese Journal of Mechanical Engineering* 31 (1) (2018) 1–8.
- [33] F. Zheng, Y. Xing, J. Jiang, B. Sun, J. Kim, M. Pecht, Influence of different open circuit voltage tests on state of charge online estimation for lithium-ion batteries, *Applied energy* 183 (2016) 513–525.
- [34] C. Lin, Q. Yu, R. Xiong, et al., A study on the impact of open circuit voltage tests on state of charge estimation for lithium-ion batteries, *Applied Energy* 205 (2017) 892–902.
- [35] S. Jiang, J. Shi, M. Borah, S. Moura, Weaknesses and improvements of the extended kalman filter for battery state-of-charge and state-of-health estimation, in: *2024 American Control Conference (ACC)*, IEEE, 2024, pp. 1441–1448.